

PCCP

Accepted Manuscript



This is an *Accepted Manuscript*, which has been through the Royal Society of Chemistry peer review process and has been accepted for publication.

Accepted Manuscripts are published online shortly after acceptance, before technical editing, formatting and proof reading. Using this free service, authors can make their results available to the community, in citable form, before we publish the edited article. We will replace this *Accepted Manuscript* with the edited and formatted *Advance Article* as soon as it is available.

You can find more information about *Accepted Manuscripts* in the [Information for Authors](#).

Please note that technical editing may introduce minor changes to the text and/or graphics, which may alter content. The journal's standard [Terms & Conditions](#) and the [Ethical guidelines](#) still apply. In no event shall the Royal Society of Chemistry be held responsible for any errors or omissions in this *Accepted Manuscript* or any consequences arising from the use of any information it contains.

Mechanistic aspects of Thioflavin-T self-aggregation and DNA binding: evidence for dimer attack on DNA grooves

A. Biancardi, T. Biver*, A Burgalassi, M. Mattonai, F. Secco, M. Venturini

Department of Chemistry and Industrial Chemistry – University of Pisa – Via Risorgimento 35 - 56126 Pisa (I)

Keywords: intercalation, groove binding, dimerization, external binding, T-jump.

* Corresponding author: tarita.biver@unipi.it

Electronic Supplementary Information (ESI) available: absorbance spectra of TFT at different dye concentration and relevant Lambert and Beer plots; molar extinction coefficient of TFT dependence on the salt content of the medium; two-component deconvolution of the fluorescence emission spectra of TFT at different dye concentrations; example of kinetic trace recorded for a solution containing TFT alone; plot of the reciprocal relaxation time vs. TFT monomer concentration; analysis of the data of the spectrophotometric titration of the TFT/DNA system according to equation (6); excitation and emission spectra and 3D contour plot of TFT and TFT/DNA; emission spectra, binding isotherm and relevant analysis according to equation (6) for a spectrofluorometric titration of TFT with DNA; example of Scatchard plot obtained from absorbance titration data for the TFT/DNA system; temperature dependence of the binding constant K for the TFT/DNA system; T-jump relaxation curves registered for the TFT/DNA system under low dye and polymer excess conditions; T-jump amplitude analysis for the fast step of the curves registered for the TFT/DNA system under low dye and polymer excess conditions; T-jump relaxation curves registered for the TFT/DNA system under high dye content conditions; derivation of equations (4)-(11)-(12)-(14) of the text and derivation of the relationship between relaxation curve amplitude and dye content.

Abstract

Thioflavin-T (TFT) is a fluorescent marker widely employed in biomedical research but the details of its binding to polynucleotides have been poorly enlightened. This paper presents a study of the mechanisms of TFT self-aggregation and binding to DNA. Relaxation kinetics of TFT solutions show that the cyanine undergoes dimerization followed by dimer isomerisation. The interaction of TFT with DNA has been investigated using static methods, as spectrophotometric and spectrofluorometric titrations under different conditions (salt content, temperature), fluorescence quenching, viscometric experiments and the T-jump relaxation method. The combined use of these techniques enabled to show that TFT monomer undergoes intercalation between the DNA base pairs and external binding according to a branched mechanism. Moreover, it has been observed that, under dye excess conditions, also the TFT dimer binds to the DNA grooves. The molecular structures of intercalated TFT and groove-bound TFT dimer are obtained by performing QM/MM MD simulations.

Introduction

Thioflavin-T (4-(3,6-dimethyl-1,3-benzothiazol-3-ium-2-yl)-N,N-dimethylaniline, TFT) is a fluorescent emicyanine dye (Figure 1) which acts as a molecular rotor.^{1, 2} Computational studies have shown that a twisted internal charge-transfer (TICT) process takes place in the excited singlet state, resulting in a transition from the fluorescent locally excited (LE) state to the non-fluorescent TICT state, accompanied by torsion angle growth from 37 to 90 degrees.³ The TICT process effectively competes with radiative transition from the LE state and is responsible for significant quenching of the dye fluorescence in low-viscosity environments.

But the interest on TFT molecule also stays in the fact that its peculiar photophysical properties can find application in biochemistry and medicine. TFT has been used as a common marker in biomedical research over the last 50 years. The ability of the TFT molecule to recognise amyloid

fibrils where other staining reagents gave inconclusive results was shown for the first time more than fifty years ago.⁴ Amyloid fibrils play a role in several pathologies connected to incorrect folding, as for instance the Alzheimer's disease.⁵ More recently, TFT has become a major tool to recognise these fibrils, both *in vivo* and *in vitro*.^{2, 6, 7} Molecular dynamics simulations have shown that TFT binds selectively to the fibrils, in particular at the level of β -sheet and at hydrophobic amino acid residues as tyrosine.⁸ This interaction, by inhibiting the rotation of the dye around its central bond, produces a strong enhancement of fluorescence emission.^{6, 7}

These observations strongly suggest that TFT could show high affinity for the inner hydrophobic region of DNA. Indeed, molecules of the cyanine family are strong intercalators⁹⁻¹¹ and TFT itself interacts with DNA.^{12, 13} Note that the TFT/DNA system has an inherent complexity due to the possible dye self-aggregation, a process known to occur for cyanine dyes^{10, 14, 15} and also for TFT.^{12, 16} On the other hand, a detailed analysis of the binding mechanism of TFT to nucleic acids is, at our knowledge, still not available. We believe that an in depth investigation of the TFT/DNA system could be of significant interest both as far as concerns the light emitting properties of the TFT molecular rotor and the understanding and optimisation of the biological/biomedical applications of this dye. On this basis, we have performed a study of the reaction mechanism of TFT auto-aggregation tendency and of its binding to natural DNA.

Results: Thioflavin-T auto-aggregation

Spectral features Absorbance spectra of TFT solutions of different concentration ($C_D = 2.0 \times 10^{-6}$ to 8.4×10^{-5} M range) were measured (Figure 1) and the linearity of absorbance vs. concentration plots was checked (Figure 1S of ESI). Differently from other cyanine dyes under similar conditions,¹⁴ no deformation of the band shape could be observed by increasing dye level and the linearity of the trends was confirmed in the explored concentration range. The dye maximum absorbance is fixed at 412 nm, in agreement with previous literature data¹² and theoretical calculations.³ The slope of the absorbance vs. concentration plots are used to evaluate

the molar extinction coefficients for the TFT dye at different wavelengths (see “Materials” paragraph). The extinction coefficient was independent of the salt content (I) of the medium (NaCl) in the 0.11 M to 2.26 M range (Figure 2S). Thus, no evidence for dye aggregation could be provided by absorbance measurements. However, as concerns fluorescence, the spectral features significantly depend on the TFT concentration (Figure 2).

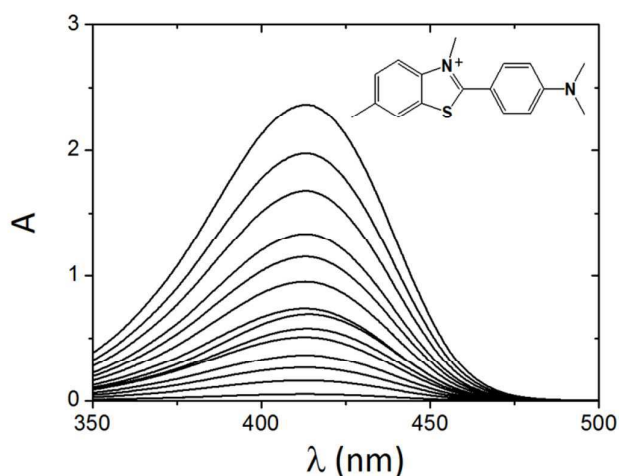


Figure 1 Absorbance spectra and structure of Thioflavin-T (TFT). $C_D = 2.0 \times 10^{-6}$ to 8.4×10^{-5} M, $I = 0.11$ M, pH 7.0.

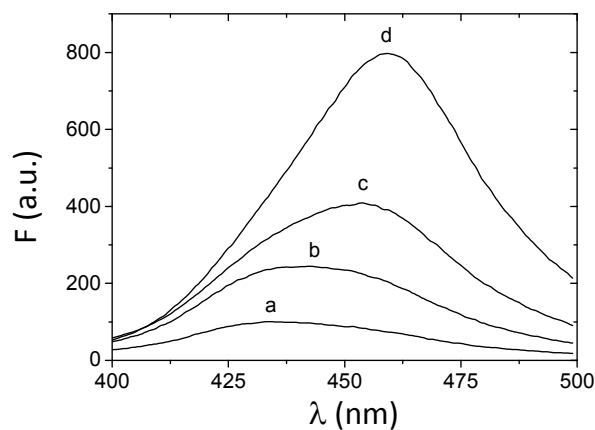


Figure 2 Fluorescence emission spectra at different TFT concentration (C_D). $C_D = 1.44 \times 10^{-6}$ M (a), 7.19×10^{-6} M (b), 3.56×10^{-5} M (c), 7.06×10^{-5} M (d), $I = 0.11$ M, pH 7.0, $\lambda_{ex} = 340$ nm, $T = 25^\circ\text{C}$.

The fluorescence emission spectra are well described by two components (Figure 3S), the first being centred at $\lambda_{em1} = 428 \pm 1$ nm, the second at $\lambda_{em2} = 453 \pm 4$ nm. The ratio of fluorescence intensities at the maxima of the two component emissions ($F(\lambda_{em1})/F(\lambda_{em2})$) decreases by increasing concentration (Figure 3S), indicating that λ_{em1} should be related to the monomer and λ_{em2} to the aggregate form. Quenching experiments on TFT using iodide gave downward curved Stern-Volmer plots (Figure 3). This result is in agreement with previous findings.¹²

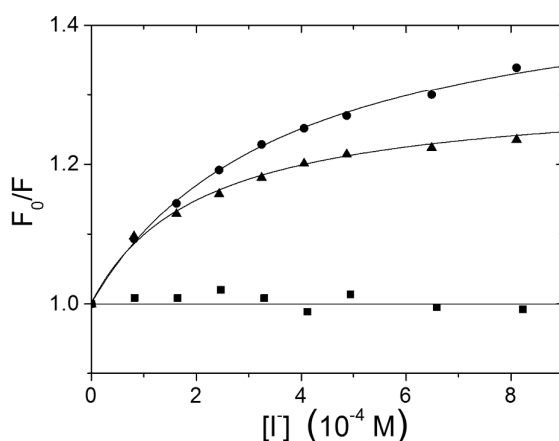


Figure 3 Stern-Volmer plots for TFT alone and for TFT/DNA system quenching by NaI, $I = 0.01$ M, pH 7.0, $\lambda_{ex} = 340$ nm, $T = 25$ °C. (●) TFT alone, $C_D = 1.5 \times 10^{-5}$ M, $\lambda_{em} = 441$ nm; (▲) TFT alone, $C_D = 1.0 \times 10^{-5}$ M, $\lambda_{em} = 441$ nm; (■) TFT + DNA, $C_D = 1.5 \times 10^{-5}$ M, $C_P = 2.0 \times 10^{-3}$ M, $\lambda_{em} = 394$ nm. The continuous lines represent the fit to equation (1).

Similar trends in complex systems (dye/vesicles, dye/biomolecules) are often fitted to a model where the fraction of accessible fluorophore is considered.¹⁷ Taking into account the monomer – aggregate equilibrium, a more general model that assumes two independent sites with different sensitivity to quenching was considered (equation (1)).¹⁸

$$\frac{F_0}{F} = \left[\frac{f_1}{(1+K_{SV1}[Q])} + \frac{f_2}{(1+K_{SV2}[Q])} \right]^{-1} \quad (1)$$

Here, f_i is the fraction of the total fluorescence relative to the i -th species and K_{SVi} the relevant quenching constant. The fit yields $f_1 = 0.324 \pm 0.007$, $K_{SV1} = (4.0 \pm 0.2) \times 10^3$ M⁻¹, $f_2 = 0.675 \pm$

0.007 and $K_{SV2} \cong 0 \text{ M}^{-1}$ for $C_D = 1.5 \times 10^{-5} \text{ M}$ and $f_1 = 0.228 \pm 0.007$, $K_{SV1} = (6.3 \pm 0.6) \times 10^3 \text{ M}^{-1}$, $f_2 = 0.770 \pm 0.006$ and $K_{SV2} \cong 3 \pm 3 \text{ M}^{-1}$ for $C_D = 1.0 \times 10^{-5} \text{ M}$.

Kinetics The kinetic experiments have been done using the T-jump technique with absorbance detection. In the explored range of dye concentrations ($C_D = 7.9 \times 10^{-6} \text{ M}$ to $3.15 \times 10^{-4} \text{ M}$) a monoexponential relaxation effect was observed (Figure 4S), which reveals the occurrence of dye auto-aggregation. It should be noted that the higher sensitivity of the kinetic method with respect to spectrophotometry enables the characterisation of the aggregation process. The mono-exponential fit of the curves provides the values of the relaxation time constant ($1/\tau$) and amplitude (ΔAbs). Their dependence on the dye content (C_D) is shown in Figure 4.

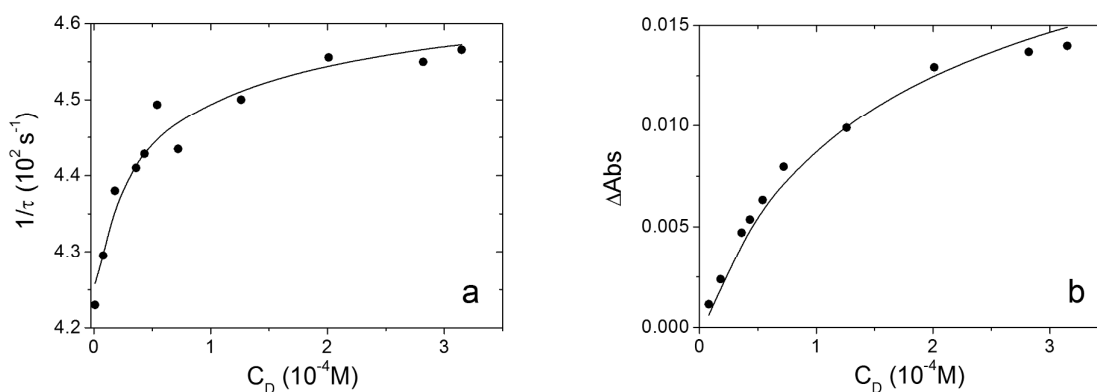


Figure 4 Reciprocal relaxation time ($1/\tau$, a) and amplitude (ΔAbs , b) of the kinetic traces as a function of the TFT concentration (C_D). $I = 0.11 \text{ M}$, $\text{pH} 7.0$, $T = 25^\circ\text{C}$. The continuous lines are the trends calculated according to the parameters values (Table 1) and equations (4) and (S4.17).

These data could not be fitted to a model that considers only TFT aggregation. The mechanism that agrees with the experimental findings is shown in equations (2) and (3) where, in addition to a fast pre-equilibrium for aggregation, here supposed to be dimerization, an isomerisation step of the formed dimer is taken into account.



Note that more complex aggregation models, as for instance the one composed by $D + D \rightleftharpoons D_2$ and $D + D_2 \rightleftharpoons D_3$ steps, were also not in agreement with the experimental trend. On the basis of the (2)-(3) model above, the relationship linking $1/\tau$ to the monomer concentration $[D]$ is given by equation (4) (for its derivation see Supplementary Information)

$$1/\tau = 4K_{\text{dim}} k_{\text{iso}}[D]/(1+4K_{\text{dim}}[D]) + k_{-\text{iso}} \quad (4)$$

where K_{dim} is the equilibrium constant of the dimerization process (2) ($K_{\text{dim}} = [D_2]/[D]^2$), k_{iso} and $k_{-\text{iso}}$ are respectively the forward and backward rate constants of the isomerisation process (3) and $[D]$ is the TFT monomer concentration. The analysis of the data points according to equation (4) has been made by setting $[D] = C_D$ as a first approximation in order to obtain a rough evaluation K_{dim} and $K_{\text{iso}} = k_{\text{iso}}/k_{-\text{iso}}$. These parameters enable to calculate $[D]$ and re-plot the data with an iterative procedure, until convergence is reached (Figure 5S). The analysis yields the reaction parameter values collected in Table 1. The K_{dim} value for TFT is similar to those obtained in case of analogous cyanine systems.^{11, 14, 19} The equation for amplitude dependence on the TFT content can also be derived (see Supplementary Information). The agreement between the experimental data and the calculated trend is very good (Figure 4b).

Table 1 Thermodynamic and kinetic parameters for TFT aggregation/isomerisation process. $I = 0.11 \text{ M}$, $\text{pH } 7.0$, $T = 25 \text{ }^\circ\text{C}$.

$K_{\text{dim}} (\text{M}^{-1})$	$K_{\text{iso}}^{\text{a}}$	$k_{\text{iso}} (\text{s}^{-1})$	$k_{-\text{iso}} (\text{s}^{-1})$
$(5.5 \pm 0.5) \times 10^3$	0.10 ± 0.01	43 ± 3	425 ± 2

$$^{\text{a}} K_{\text{iso}} = k_{\text{iso}}/k_{-\text{iso}}$$

The values of Table 1 can be used to obtain a distribution diagram for TFT in the different forms (Figure 5). This graph shows that, under the conditions of the spectroscopic experiments ($C_D \leq 8.4 \times 10^{-5} \text{ M}$) the monomer form is predominant.

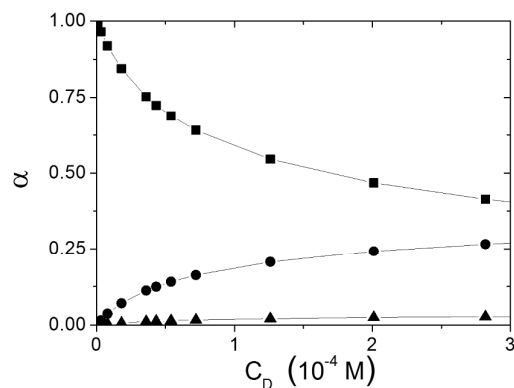


Figure 5 Distribution diagram for TFT in its different forms depending on the total dye molar concentration (C_D); α_D = monomer fraction (\blacksquare), α_{D2} = dimer fraction (\bullet), $\alpha_{D2'}$ = isomerised dimer fraction (\blacktriangle), $I = 0.11$ M, pH 7.0, $T = 25^\circ\text{C}$.

Results: Thioflavin-T binding to DNA

Spectrophotometric titrations Figure 6a shows the absorbance spectra recorded during a titration where increasing amounts of DNA are added to a TFT solution.

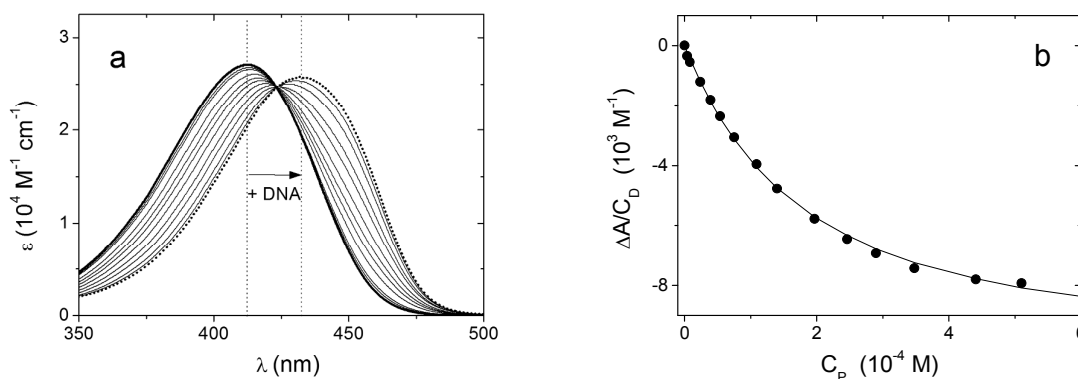


Figure 6 Absorbance features of a titration where increasing amounts of DNA are added to a TFT solution (a) and relevant binding isotherm at $\lambda = 412$ nm (b). $C_D = 5.2 \times 10^{-5}$ M, $C_P = 0$ M (—) to 5.1×10^{-4} M ($\bullet\bullet\bullet$), $I = 0.01$ M, pH 7.0, $T = 25^\circ\text{C}$. The line in (b) is the calculated trend.

The significant variation of the absorbance occurring upon increasing the DNA content (hypochromicity and bathochromic shift from 412 nm to 432 nm) and the presence of an isosbestic point indicate that the binding does take place.²⁰ This interaction can be, in a first approximation, described by reaction (5)

$$P_f + D_f \rightleftharpoons PD_{\text{tot}} \quad (5)$$

where P_f is a free binding site on DNA, D_f is the free TFT and PD_{tot} is the total complex formed. Note that equation (5) should be intended as an apparent equilibrium that can enclose more steps (see below). The titration data are plotted according to the binding isotherm shown in Figure 6b and analysed according to equation (6),¹¹ where C_P and C_D are respectively the total DNA and TFT concentrations, $\Delta A = A - \epsilon_D C_D$ is the absorbance signal change, $\Delta \epsilon = \epsilon_{PD} - \epsilon_D$ is the amplitude of the isotherm and K is the equilibrium constant associated to equation (5).

$$\frac{C_P C_D}{\Delta A} + \frac{\Delta A}{(\Delta \epsilon)^2} = \frac{1}{\Delta \epsilon} (C_P + C_D) + \frac{1}{K \Delta \epsilon} \quad (6)$$

As $\Delta \epsilon$ value is not exactly known, an iterative procedure is needed that first disregards the $\Delta A / \Delta \epsilon^2$ term and then calculates it iteratively. At convergence, the value of the equilibrium constant, K , for equilibrium (5) is calculated by the ratio slope/intercept of the straight line interpolating data points on a $(C_P C_D / \Delta A + \Delta A / \Delta \epsilon^2)$ vs. $(C_P + C_D)$ plot (Figure 6S). At 25°C and $I = 0.01$ M, $K = (7.1 \pm 0.4) \times 10^3 \text{ M}^{-1}$ and $\Delta \epsilon (\lambda = 412 \text{ nm}) = (-1.0 \pm 0.2) \times 10^4 \text{ M}^{-1} \text{ cm}^{-1}$.

Spectrofluorometric titrations The fluorescence emission properties of the TFT/DNA complex significantly differ from those of free TFT. In the absence of DNA TFT is a weak light emitter (quantum yield 10^{-4})¹ with maximum excitation and emission at 340 nm and 450 nm respectively (Figure 7S), owing to the unrestricted movement of the molecule around its central bond. Addition of DNA causes the appearance of a new emission band at $\lambda_{\text{em}} = 484$ nm with maximum excitation at $\lambda_{\text{ex}} = 450$ nm (Figure 8S) and the dramatic enhancement of the fluorescence signal (in agreement with the more restricted environment). The significant shifts of the maxima ($\Delta \lambda_{\text{em}} = 34$ nm and $\Delta \lambda_{\text{ex}} = 110$ nm) reflect a dramatic change in the dye energy features, as observed for the binding of TFT to amyloid fibrils; all changes being ascribed to motion freezing.⁶

Spectrofluorometric titrations were carried out by adding increasing amounts of DNA to TFT in the spectrofluorometric cell. The titration data were analysed in the same way of absorbance,

substituting to ΔA and $\Delta \epsilon$ in equation (6) the analogous parameters ΔF and $\Delta \phi$. Note that, under the conditions of experiments, the inner filter effect²¹ is negligible. The obtained fluorescence emission spectra, the binding isotherm and relevant analysis are shown in Figure 9S. At 25°C and $I = 0.01$ M, $K = (7.9 \pm 0.5) \times 10^3 \text{ M}^{-1}$ and $\Delta \phi = (1.3 \pm 0.4) \times 10^8 \text{ M}^{-1}$ ($\lambda_{\text{ex}} = 450 \text{ nm}$, $\lambda_{\text{em}} = 484 \text{ nm}$). The agreement between the equilibrium constants K obtained with the two methods is very good.

Salt dependence of equilibria Being TFT a positively charged dye, a dependence on the salt content of the equilibrium binding features to negative DNA is expected. Hence, absorbance and fluorescence titrations were performed in the presence of NaCl amounts ranging between 0.01 M and 0.51 M. Figure 7 shows in a dilogarithmic plot the dependence of the equilibrium constant K on the salt content (equation (7)).²²

$$\log K = \log K_0 + 0.88 m' p[\text{Na}^+] \quad (7)$$

In equation (7) K_0 is defined as the binding constant in the absence of electrostatic effect and m' is the number of sodium ions displaced from DNA by the binding of one dye molecule. Interestingly, two well defined and significantly different trends are present, depending on the technique used to measure the equilibrium constant, K . Fluorescence data depend more on the salt content, with $m'_{\text{fluo}} = 0.99 \pm 0.04$ ($\log K_0 = 2.2 \pm 0.1$), whereas for absorbance $m'_{\text{abs}} = 0.38 \pm 0.05$ ($\log K_0 = 3.3 \pm 0.1$).

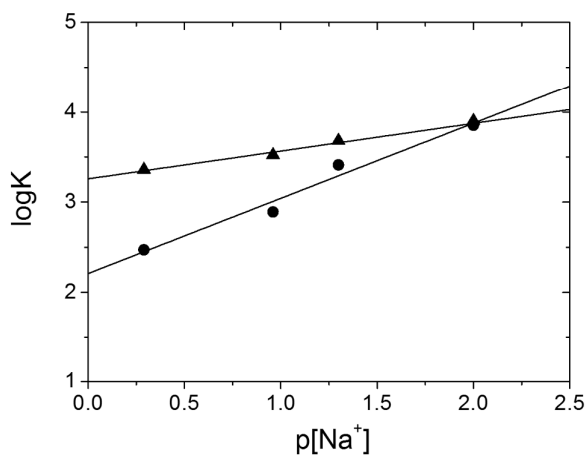


Figure 7 Dependence of the equilibrium constant, K , for the binding of TFT to DNA on the salt content of the medium (NaCl). (▲) Absorbance, (●) fluorescence, pH 7.0, $T = 25$ °C.

This result confirms the complexity of the system, where two binding modes (at least) seem to compete.

Table 2 shows the values of the $\Delta\epsilon$ parameter obtained by the absorbance titrations ($\lambda = 412$ nm) at different ionic strengths. It can be noted that the absolute value of $\Delta\epsilon$ decreases as the salt content increases. As $\Delta\epsilon = \epsilon_{PD} - \epsilon_D$ and ϵ_D do not noticeably vary with I (Figure 2S), this result indicates that higher salt favours a binding mode where the spectroscopic features of the PD complex are less different from those of free dye.

Table 2 Values of the $\Delta\epsilon$ parameter obtained by absorbance titrations of the TFT/DNA system at different ionic strengths (NaCl); pH 7.0, $\lambda = 412$ nm, T = 25°C.

I (M)	0.01	0.05	0.11	0.51
$-\Delta\epsilon$ ($M^{-1}cm^{-1}$)	$(1.0\pm 0.2)\times 10^4$	$(7.2\pm 0.2)\times 10^3$	$(2.1\pm 0.3)\times 10^3$	$(1.8\pm 0.1)\times 10^3$

The data of the spectrophotometric titrations under different salt content were analysed also using the model from Scatchard.²³ On the basis of this model, the data can be plotted according to equation (8) (see Figure 10S for an example)

$$r/[D] = K_{SC}/\gamma - K_{SC}\times r \quad (8)$$

where r is defined as the polynucleotide saturation degree ($r = [PD]/C_P = \Delta A/(\Delta\epsilon C_P)$), $[D]$ is the free dye, and γ is a parameter connected to the site size, n ($n = \frac{1}{2}(1+1/\gamma)^{24}$). The site size is the number of adjacent base pairs of the polynucleotide that, under saturation conditions, is inhibited to further react with the dye because of the interaction with a first dye molecule. Table 3 collects the values obtained by data analysis according to equation (8) and shows that a noticeable site size increase is observed by increasing the salt content of the medium.

Table 3 Values of K_{SC} and site size (n) parameters for the TFT/DNA system, obtained by the analysis of the absorbance titrations according to Scatchard (equation (8)); pH 7.0, T = 25°C.

I (M)	0.01	0.05	0.11	0.51
$K_{SC} (M^{-1})$	$(1.7 \pm 0.1) \times 10^4$	$(1.4 \pm 0.2) \times 10^4$	$(1.0 \pm 0.2) \times 10^4$	$(1.4 \pm 0.4) \times 10^4$
n	1.5 ± 0.1	1.8 ± 0.1	2.1 ± 0.3	2.9 ± 0.5

Temperature dependence of equilibria The equilibria of the TFT/DNA system have been analysed also by varying temperature in the 9°C to 36°C range (higher temperatures produced system instability). Again, the dependence on temperature of the K values is distinct for fluorescence data respect to absorbance (Figure 11S). Assuming that ΔH and ΔS are constant in the limited temperature range explored, data can be fitted according to the equation $\ln K = -\Delta H/RT + \Delta S/R$. From fluorescence data it is obtained that $\Delta H_{flu} = (-8.5 \pm 0.7) \text{ Kcal mol}^{-1}$ and $\Delta S_{flu} = (-11 \pm 2) \text{ cal mol}^{-1} \text{ K}^{-1}$, for absorbance $\Delta H_{abs} = (-3.7 \pm 0.7) \text{ Kcal mol}^{-1}$ and $\Delta S_{abs} = (5 \pm 2) \text{ cal mol}^{-1} \text{ K}^{-1}$.

Fluorescence quenching experiments To obtain information on dye protection upon DNA binding, quenching experiments were done by addition of increasing iodide (NaI) amounts to a constant dye concentration. The experiments were performed on the TFT/DNA system ($C_D = 1.5 \times 10^{-5} \text{ M}$, $C_P = 2.0 \times 10^{-3} \text{ M}$) and on TFT alone ($C_D = 1.5 \times 10^{-5} \text{ M}$), as a reference (see above). Excess of polymer concentrations and low ionic strength conditions ($I = 0.01 \text{ M}$) were chosen so to ensure quantitative formation of the complex and consequent absence of free TFT dye. The resulting Stern-Volmer plots are shown in Figure 3. In the absence of DNA, the TFT dye is strongly quenched by iodide but, in the presence of DNA, the quenching effect is no longer observed.

Viscosity measurements Viscosity measurements are often intended as the less ambiguous tool to verify the features of a small molecule binding to polynucleotides.²⁵ In fact, interaction can modify the chain length and viscosity is proportional to the cube of this length (in the rigid rod approximation²⁶). In this series of experiment the polymer concentration, C_P is kept constant

(2.6×10^{-4} M) and C_D is varied in the $C_D/C_P = 0.05 \div 0.45$ range. The relative viscosity, η/η_0 , is calculated as

$$\frac{\eta}{\eta_0} = \frac{(t - t_{\text{solv}})}{(t_{\text{DNA}} - t_{\text{solv}})} \quad (9)$$

where t , t_{solv} and t_{DNA} denote respectively the flow time of the sample (TFT/DNA mixture), of the solvent (0.01 M NaCac) and of solvent + DNA 2.6×10^{-4} M. The plot of Figure 8 shows the dependence of $(\eta/\eta_0)^{1/3}$ on C_D/C_P .

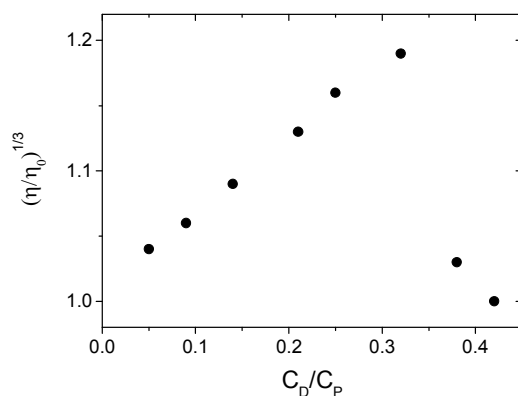


Figure 8 Dependence of the relative viscosity $(\eta/\eta_0)^{1/3}$ on the ratio C_D/C_P for the TFT/DNA system. $C_P = 2.6 \times 10^{-4}$ M, $I = 0.01$ M, pH 7.0, $T = 25$ °C.

The significant increase of $(\eta/\eta_0)^{1/3}$ corroborates a strong TFT binding to DNA. On the other hand, the abrupt change of the viscosity at $C_D/C_P \cong 0.3$ confirms the non-simple binding features of the TFT/DNA system.

Kinetic analysis at low dye loading ($C_D/C_P < 0.45$) The T-jump measurements on the TFT/DNA system have been performed in the absorbance mode at the same wavelength (450 nm) and under the experimental conditions of the dye aggregation experiments. Under conditions of very low dye content ($C_D = 2.0 \times 10^{-6}$ M), where dye self-aggregation is negligible, and in the presence of DNA excess ($C_D/C_P = 0.005 \div 0.45$) two kinetic effects of opposite amplitude and differing in the time scale for more than one order of magnitude were observed (Figure 12S). The

traces have been fitted to a bi-exponential equation that yields the amplitudes and reciprocal relaxation times of the two effects. The presence of two distinct kinetic effects (fast and slow) indicates that the “PD_{tot}” notation (equation (5)) includes two different complex forms (PD and PD'), i.e. that equation (5) can be expanded as in scheme (10).



The reciprocal relaxation times of the fast ($1/\tau_f$) and slow ($1/\tau_s$) effects are plotted against the reactant content $[P]+[D]$ (Figure 9). Here, $[P]$ (free polymer) and $[D]$ (free dye) are calculated using, in a first approximation, the equilibrium constant K from thermodynamics and then the K obtained from a combination of kinetic parameters (see below), using an iterative procedure which is repeated until convergence.

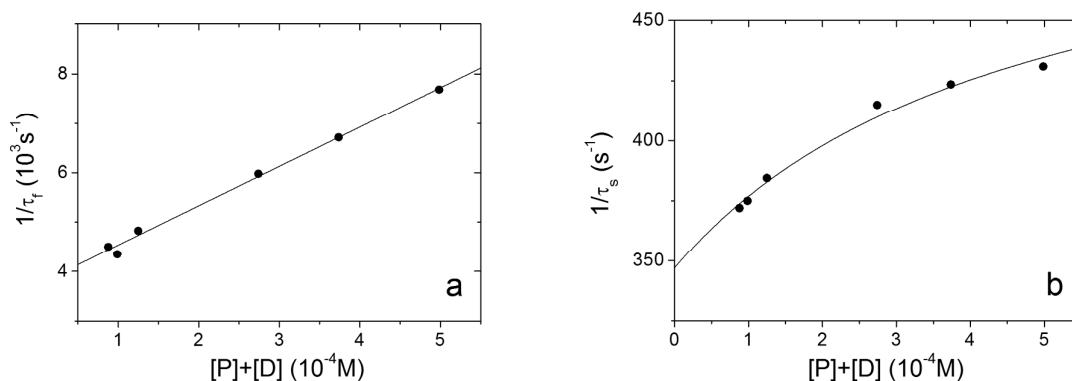


Figure 9 Reciprocal fast ($1/\tau_f$, a) and slow ($1/\tau_s$, b) relaxation times dependence on the reactant content $[P]+[D]$ for the TFT/DNA system at low dye content and under DNA excess conditions. $I = 0.11\text{ M}$, $\text{pH } 7.0$, $T = 25\text{ }^\circ\text{C}$. The continuous lines are data fit to equations (11) and (12) respectively.

The dependence of the reciprocal fast relaxation time, $1/\tau_f$, on the concentration variable is linear (Figure 9a), according to equation (11).

$$1/\tau_f = k_f([P]+[D]) + k_{-f} \quad (11)$$

The concentration dependence of the reciprocal slow relaxation time, $1/\tau_s$, tends to a plateau (Figure 9b) in agreement with equation (12)

$$1/\tau_s = k_s([P]+[D])/(1 + K_f([P]+[D])) + k_{-s} \quad (12)$$

where $K_f = k_f/k_{-f}$. Equations (11) and (12) are derived on the basis of scheme (10) (see Supplementary Information), that also yields $K = K_f + K_s = (k_f/k_{-f}) + (k_s/k_{-s})$. Table 4 collects the results obtained; the values of K obtained as ratios of the kinetic constants (absorbance mode) agree with those evaluated from equilibria (absorbance mode).

Table 4 Reaction parameters for the interaction of DNA with TFT. I = 0.11 M, pH 7.0, T = 25°C.

$10^{-3}K$	$10^{-3}K_f$	$10^{-3}K_s$	$10^{-4}K_3$	$10^{-6}k_f$	$10^{-3}k_{-f}$	$10^{-5}k_s$	$10^{-2}k_{-s}$
(M ⁻¹)	(M ⁻¹)		(M ⁻¹)	(M ⁻¹ s ⁻¹)	(s ⁻¹)	(s ⁻¹)	(s ⁻¹)
3.2±0.2 ^a	2.1±0.1 ^c	0.77±0.01 ^e	1.0±0.3 ^g	8.0±0.3 ^f	3.7±0.1 ^f	3.6±0.2 ^f	3.5±0.1 ^f
2.8±0.5 ^b	2.6±0.5 ^d	1.1±0.1 ^f				8.8±1.1 ^g	8.0±1.1 ^g

(^a) Kinetics $K = K_f + K_s = (k_f/k_{-f}) + (k_s/k_{-s})$; (^b) thermodynamics – absorbance; (^c) $K_f = k_f/k_{-f}$; (^d) amplitude analysis; (^e) thermodynamics – fluorescence; (^f) low-dye kinetic analysis, $K_s = k_s/k_{-s}$; (^g) high-dye kinetic analysis, $k_{-s} = k_s/K_s$.

The relaxation amplitude of the fast effect was analysed according to equation (13).²⁷

$$\sqrt{\frac{C_D C_P}{\delta A}} = \frac{\sqrt{RT^2}}{\sqrt{K_f \Delta \epsilon_f \Delta H_f \delta T}} + \frac{K_f C_P \sqrt{RT^2}}{\sqrt{K_f \Delta \epsilon_f \Delta H_f \delta T}} \quad (13)$$

Here δA is the amplitude of the relaxation effect (expressed as a change of absorbance) following a jump of temperature of magnitude δT (2.7 °C), R is the gas constant, ΔH_f is the enthalpy variation associated to the fast step, and $\Delta \epsilon_f$ the relevant extinction coefficient variation (ΔH_f and $\Delta \epsilon_f$ are

unknown). The plot of $(C_D C_P)/\delta A^\circ)^{1/2}$ vs. C_P is linear (Figure 13S) and the ratio slope/intercept provides the value of K_f also reported in Table 4. A very good agreement is found between the K_f values obtained by the two different calculations.

Kinetic analysis at high dye loading ($C_D/C_P > 0.8$) A set of T-jump experiments was done at high dye content ($C_D > 6.0 \times 10^{-5}$ M) and C_D/C_P ranging between 0.80 and 3.3. Under these circumstances dye dimerization can no longer be neglected. Two kinetic effects of opposite amplitude and differing in the time scale by one order of magnitude have been detected (Figure 14S). Despite the qualitative similarity with the curves obtained in the case of the low dye content experiments, the two sets of experiments could not be plotted together with respect to concentration variable, as the two data sets exhibit distinct trends. This result indicates that the reaction mechanism active here does not coincide with scheme (10). The fit of the relaxation curves provides the amplitudes and the reciprocal relaxation times of the fast ($1/\tau'_f$) and slow ($1/\tau'_s$) effects. The time constant of the slow effect ($1/\tau'_s \cong 70$ s⁻¹) was found to be independent of reactant concentrations; hence, the slow effect was attributed to a polynucleotide rearrangement upon previous dye binding and was no longer investigated. On the contrary, $1/\tau'_f$ depends on the reactant concentration as shown in Figure 10.

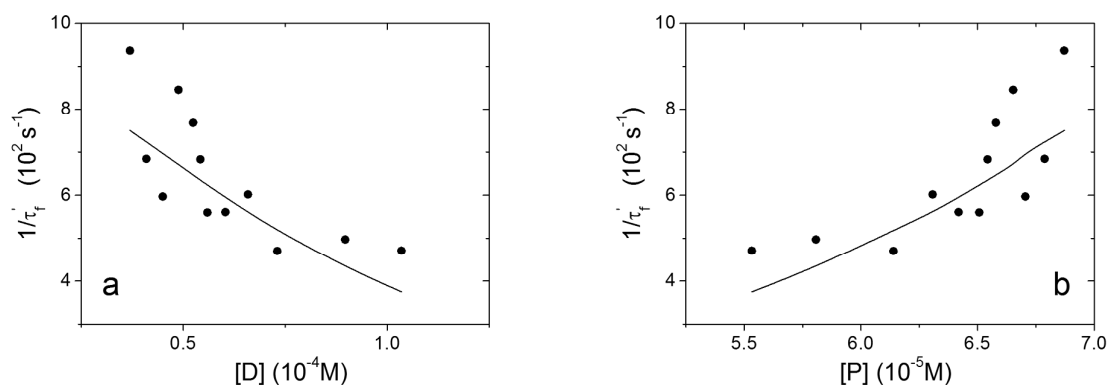


Figure 10 Reciprocal fast ($1/\tau'_f$) relaxation times dependence on the reactant content for the TFT/DNA system at high dye content. $I = 0.11$ M, pH 7.0, $T = 25$ °C. The continuous lines are data fit to equation (15).

Among the several models tested, the one that reproduces the experimental results is shown in scheme (14).



In this mechanism, additional steps are present respect to scheme (10) because of the non-negligible dimer content in the system. The formation of PD (slow) is supposed to be rate determining, whereas the other steps are fast. On this basis, the dependence of $1/\tau'_f$ on the reactant content corresponds to equation (15) (for derivation see Supplementary Information).

$$1/\tau'_f = \frac{k_s([P] - \mu \times [D]) + k_{-s} \frac{\varepsilon}{\theta}}{K_f([P] - \mu \times [D]) + 1 + 4[D]K_{\text{dim}}} \quad (15)$$

where $[P]$ and $[D]$ are free polymer and dye respectively, $\mu = (\beta/\alpha) - (\gamma/\alpha) \times (\varepsilon/\theta)$, $\varepsilon = 1 + (\beta/\alpha) + 4[D]K_{\text{dim}} + 4K_3K_sK_{\text{dim}}[P] \times [D]^2$, $\theta = (\gamma/\alpha) + 2K_3K_{\text{dim}}[D]^2$, $\gamma = 1 + K_3K_{\text{dim}}[D]^2$, $\beta = K_f[P] + 2K_3K_sK_{\text{dim}}[P] \times [D]^2$, $\alpha = 1 + K_f[D]$. The analysis requires an iterative procedure where, in a first approximation, $[P] = C_p$, $[D] = C_D$ and $[PD] = 0$. In the subsequent steps $[P]$, $[D]$ and $[PD]$ are calculated from K_f , K_{dim} and the K_3 value obtained, until convergence is reached (see Supplementary Information). Note that $K_f = 2.1 \times 10^3 \text{ M}^{-1}$ (Table 4) and $K_{\text{dim}} = 1.6 \times 10^3 \text{ M}^{-1}$ (Table 1) are known under the conditions of experiments. The parameters to be optimised were set to two (k_s and K_3) as for k_{-s} we used the relationship $k_{-s} = k_s/K_s = k_s/1.1 \times 10^3$ (Table 4). The values of k_s and K_3 which simultaneously fit the data of Figs. 10a and 10b are collected in Table 4. Taking into account the complexity of the system, the agreement between k_s values obtained by the two kinetic series should be considered good.

Discussion

TFT self-aggregation TFT underwent self-aggregation, similarly to other dyes of the cyanine family. However, TFT aggregation process showed some peculiar aspects.

First of all, no spectrophotometric evidence of the aggregation phenomenon was obtained in a concentration range where analogously aggregating cyanine dyes showed significant absorbance spectra deformation.^{11, 14} This means that the absorbance spectral characteristics of the dye dimer are rather similar to those of dye monomer. Nevertheless, the spectrofluorometric and t-jump approaches enabled to enlighten TFT self-aggregation owing to their higher sensitivity compared to classical spectrophotometry.

Second, a more complex aggregation mechanism had to be considered respect to other similar systems. In fact, the kinetic data on TFT could not be fitted on the basis of a simple dimerization model. An additional isomerisation step was necessary to explain the experimental behaviour. Cyanine dyes can undergo both J-aggregation or H-aggregation,^{11, 15, 28} where the former process gives rise to structures with large offset (more abundant in the literature) and the latter to co-facial forms with little offset. J-aggregates can be distinguished from H-aggregates on the basis of the position of the dimer absorption band respect to the monomer,²⁹ but this distinction is impossible for TFT, due to the above presented reasons. The two dimers, D_2 and D_2' , correspond probably to forms with different offset, but more important variation of their reciprocal orientation cannot be excluded. The proper structural definition of the dimer forms was beyond the scope of the present manuscript and will be better analysed in the future, with the aid of theoretical calculations.

As regards TFT fluorescence quenching experiments, the analysis assuming two independent sites with different sensitivity (monomer and aggregate) shows that one of the two sites displays little or even no sensitivity to the quencher. The contribution of the species with no sensitivity to the quencher increases by lowering the dye content. This means that it is the dye monomer that is not quenched. Dye rotation can likely account for loss of interaction with iodide. The ϕ_{D_2}/ϕ_D ratio can be evaluated using the data fit according to equation (1). Under the conditions of experiment ($I =$

0.01M, $T = 25\text{ }^\circ\text{C}$), $K_{\text{dim}} = 3.8 \times 10^3\text{ M}^{-1}$ (obtained by transforming the datum at $I = 0.11\text{M}$ in Table 1 by means of the Güntelberg equation).³⁰ Moreover, $[D] = 0.90 \times C_D$ (at $C_D = 1.5 \times 10^{-5}\text{ M}$) or $[D] = 0.93 \times C_D$ (at $C_D = 1.0 \times 10^{-5}\text{ M}$). The relationships $f_1 = f_{D2} = \varphi_{D2}[D_2]_{\text{tot}} / (\varphi_D[D] + \varphi_{D2}[D_2]_{\text{tot}})$ and $f_2 = f_D = \varphi_D[D] / (\varphi_D[D] + \varphi_{D2}[D_2]_{\text{tot}})$ also apply, with $[D_2]_{\text{tot}} = [D_2] + [D_2']$. It can thus be calculated that $\varphi_{D2} = 8.6 \times \varphi_D$ ($C_D = 1.5 \times 10^{-5}\text{ M}$) or $\varphi_{D2} = 7.9 \times \varphi_D$ ($C_D = 1.0 \times 10^{-5}\text{ M}$). These results agree with the increase of fluorescence emission upon aggregation, due to motion restriction. Note, however, that the downward curvature of the Stern-Volmer plot could also be due to the two different locally excited (LE) and twisted intramolecular charge transfer (TICT) TFT excited states.^{31 3}

TFT binding to DNA Different binding modes were found to be operative in the TFT/DNA system. The measured binding constant is an apparent parameter which takes into account two different binding modes. Different experimental conditions and/or methods put into evidence the two modes to a different extent. The results suggest that, under conditions of low dye content and low ionic strength, an intercalative binding prevails. Under low added salt conditions, intercalation is largely majority and the equilibrium constant values, measured using different techniques, display good agreement. By increasing the salt content, this binding mode was better evidenced by the fluorescence measurements, as this technique enables lower dye concentrations be used and intercalation likely produces more significant changes in the light emission characteristics of the dye (motion strongest inhibition). Intercalation of TFT within polynucleotide base pairs was confirmed: (A) by the $m' = 0.99$ value of the fluorescence salt dependence analysis (close to total +1 charge of TFT); (B) by the site size value at low salt content, $1 < n < 2$ (in agreement with the excluded site model for intercalation³²); (C) by the values of ΔH_{flu} ($-8.5\text{ Kcal mol}^{-1}$ i.e. highly negative) and $\Delta S_{\text{flu}} = (-11\text{ cal mol}^{-1}\text{ K}^{-1}$ i.e. highly negative) that, according to Chaires³³, agree with intercalation; (D) by the total absence of quenching phenomena at $I = 0.01\text{M}$ (in agreement with a dye inaccessibly buried in the polynucleotide); (E) by the significant increase of the relative viscosity of the system for $C_D/C_P < 0.3$ (intercalation is the binding mode that produces the most

important changes in the polymer length²⁵). The molecular structure of TFT intercalated in double stranded DNA, obtained performing a QM/MM MD simulation, is shown in Figure 11.

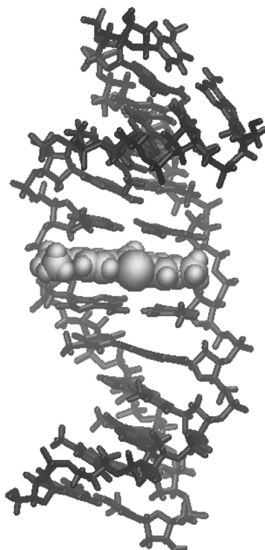


Figure 11. Molecular structure of a TFT dye molecule intercalated in DNA, obtained performing a QM/MM MD simulation.

The second binding mode, detected mainly in the absorbance experiments and when the salt and/or the dye content was increased, is more difficult to classify. However, the results suggest that this could be an external binding. This hypothesis is supported by the following observations: (A) the analysis of salt dependence of absorbance data on equilibria yields $m' = 0.38$, thus TFT electrostatic effect in this mode is significantly less than expected on the basis of the reactants charges, thus suggesting a weaker and external interaction, weaker than intercalation; (B) the values of $\Delta\varepsilon = \varepsilon_{PD} - \varepsilon_D$ decrease by increasing ionic strength, indicating that salt addition favours a weaker binding mode, less influencing the photophysical properties of the dye upon binding; (C) the site size rises until $n \cong 3$ on rising the ionic strength; (D) the value of ΔH_{abs} ($-3.7 \text{ Kcal mol}^{-1}$) is small and that of ΔS_{abs} is positive ($+5 \text{ cal mol}^{-1} \text{ K}^{-1}$)³³; (E) the viscosity trend exhibits an abrupt change at $C_D/C_P > 0.3$ that reveals that the increase ascribed to intercalation stops and is even lost.

Figure 12 shows the QM/MM calculated molecular structure of a minor groove bound dimer. The QM/MM molecular structures shown in Figures 11 and 12 confirm the robustness of the proposed mechanism. The QM/MM calculations seem to be promising in achieving a better understanding of the TFT-DNA interaction and the relevance of these findings will require further investigations.

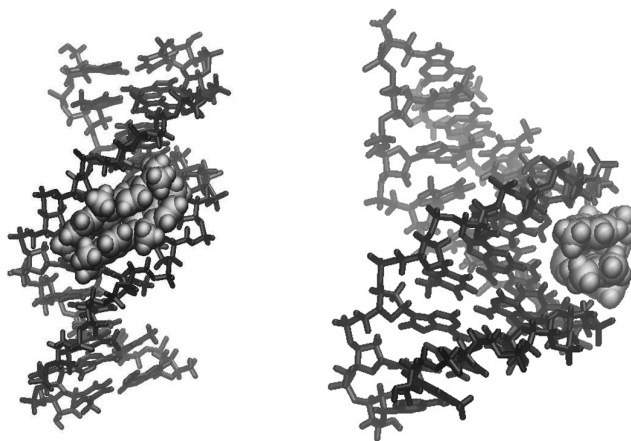


Figure 12. Molecular structures of a minor groove bound TFT dimer, obtained by performing a QM/MM MD simulation.

Mechanistic aspects of TFT binding to DNA at low dye loading The kinetic study enabled an enlightenment of the details of the binding processes. The analysis of the system was done first under conditions that strongly repress dye aggregation, both in solution and on the polynucleotide (low dye content and high DNA excess). The two kinetic effects found are explained on the basis of the branched mechanism shown in scheme (10), that considers the parallel, mutually exclusive formation of two different PD' and PD complex forms. The direct transfer mechanism proposed for the ethidium/DNA system³⁴ can be discarded here since it requires that the plot of $(1/\tau_f \times 1/\tau_s)$ vs. $[P]+[D]$ would display a parabolic trend,³⁵ contrary to our findings. On the other hand, a series mechanism as in scheme (16) is not kinetically distinguishable from scheme (10).¹¹



However, this could also be discarded, as it produced numerical values that could not find any agreement with the possible models for the high dye content experiments. Exploring the details of the model presented in scheme (10), it can be observed that the values of k_f and k_s found for this system ($k_f = 8.0 \times 10^6 \text{ M}^{-1}\text{s}^{-1}$ and $k_s = 3.6 \times 10^5 \text{ M}^{-1}\text{s}^{-1}$) are too low for a diffusive process ($k_{\text{dif}} > 10^8 \text{ M}^{-1}\text{s}^{-1}$ ³⁶). So a first step should be considered, leading to the diffusion controlled formation of an outer complex (P,D) that will evolve to the PD' and PD forms (reaction scheme (17), $k_f = K_0 \times k_f'$, $k_s = K_0 \times k_s'$).



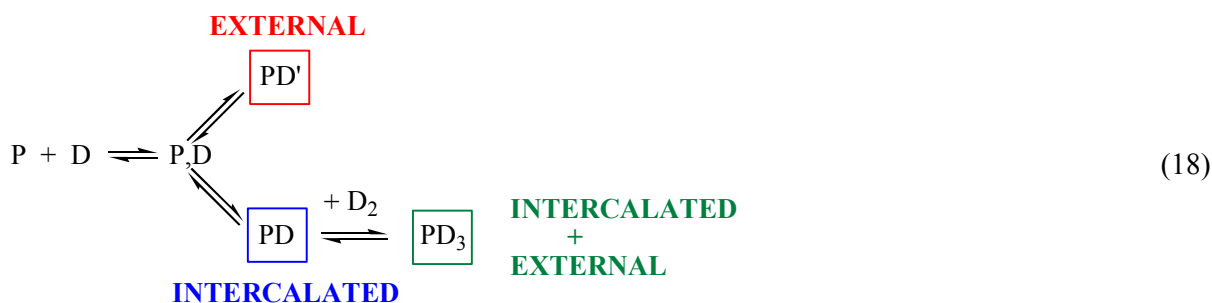
This hypothesis is confirmed also by the values of the thermodynamic parameters. In fact, K_f and K_s are too high to concern formation of an electrostatic outer complex ($K_f = 2.1 \times 10^3 \text{ M}^{-1}$ and $K_s = 1.1 \times 10^3 \text{ M}^{-1}$ against a value that, for a mono-positive dye forming an electrostatic complex at $I = 0.11\text{M}$, should not exceed 10^2 M^{-1} ³⁷).

The PD' and PD forms cannot be exactly defined in their structures. Nevertheless, the results obtained by the binding equilibria analysis indicated that two types of binding, intercalation and external, should be taken into account. Under such a hypothesis, PD should be the intercalated species and PD' the groove bound one. In fact, intercalation requires energy barriers to be overcome that account for the lower rate of dye penetration into base pair slots. The numerical values of the binding parameters for the slow step given in Table 4 are in agreement with those found for similar intercalating systems.^{14, 38} On the other hand, external binding is fast and agrees with the high rate constant found for the fast step ($k_f = 8.0 \times 10^6 \text{ M}^{-1}\text{s}^{-1}$).³⁶

Mechanistic aspects of TFT binding to DNA at high dye loading Under conditions of high TFT content, the mechanism of scheme (14) appears to be the most suitable in order to depict the TFT/DNA system features. In effect, several other mechanisms have been taken into account and, among them, the one where the $PD + D_2 \rightleftharpoons PD_3$ step was replaced by $PD + D \rightleftharpoons PD_2$. However, none of the models other than that of scheme (14) was able to reproduce the experimental behaviour. The inclusion of D_2' in models as scheme (14) produces negligible effects as this species is largely minority. In scheme (14) $P + D \rightleftharpoons PD$ is the rate-determining step, whereas other equilibria are fast. Here a pre-formed TFT-TFT dimer (D_2) is able to bind DNA in a polymer section where some dye molecules are already intercalated (PD), leading to formation of a both intercalated and externally bound species (PD_3). This “crowded” situation is made possible by the conditions of high dye loading. In the PD_3 form, the D_2 dimer could be bound to a DNA groove. In fact, the existence of a TFT/DNA complex form where a dimer inserts itself into the polymer groove was already advanced by other authors.¹² Moreover, the high affinity of TFT for DNA cavities has been very recently documented.³⁹

Conclusions

As concerns TFT self-aggregation, an unusual isomerisation reaction of dye dimer was found to take place. In the case of DNA binding, similarly to other small molecule/polynucleotide systems⁴⁰, each approach was differently sensitive to a particular aspect of the investigated process. This strengthens that multiple techniques are needed to obtain a comprehensive picture of such complicate systems. Small molecules can interact with polynucleotides simultaneously by intercalation and groove binding: this is accepted in principle but has been infrequently demonstrated in real systems. In the here investigated TFT/DNA system, under condition of high dye content and non-negligible TFT dimerization, formation of a simultaneously intercalated and groove bound complex is likely to occur. On the whole, the proposed mechanism is shown below (scheme (18)).



Acknowledgements Financial support of “Obra Social La Caixa” is gratefully acknowledged.

Materials and methods

Materials Thioflavin-T (4-(3,6-dimethyl-1,3-benzothiazol-3-ium-2-yl)-N,N-dimethylaniline, from now on TFT) was purchased by AAT Bioquest in the form of chloride salt (purity $\geq 99.8\%$). Stock solutions of the dye (2×10^{-3} M) were prepared by dissolving weighed amounts of the solid in DMSO (Carlo Erba, purity $\geq 99.5\%$) and kept in the dark at 4°C . Working solutions were obtained by dilution of the stocks to such a level that the DMSO content could be neglected. In the case of viscosity experiments the solid was dissolved directly in water and used within 2 days. The stock concentration was also checked spectrophotometrically, using the molar extinction coefficients measured in this work ($\epsilon^{385} = (1.80 \pm 0.01) \times 10^4 \text{ M}^{-1}\text{cm}^{-1}$ at $\lambda = 385 \text{ nm}$, $\epsilon^{412} = (2.82 \pm 0.01) \times 10^4 \text{ M}^{-1}\text{cm}^{-1}$ at $\lambda = 412 \text{ nm}$, $\epsilon^{435} = (1.89 \pm 0.01) \times 10^4 \text{ M}^{-1}\text{cm}^{-1}$ at $\lambda = 435 \text{ nm}$; $I = 0.1 \text{ M}$ (NaCl), pH 7.0). The molar concentration of the TFT dye is denoted as C_D . Calf thymus DNA (from now on DNA) was purchased from Sigma-Aldrich in the form of lyophilised sodium salt, dissolved into water and sonicated to reduce the polynucleotide length (to ca. 500 base pairs) following an already described procedure.⁴¹ Stock solutions were standardised spectrophotometrically, using $\epsilon = 13200 \text{ M}^{-1}\text{cm}^{-1}$ at 260nm, $I = 0.1 \text{ M}$ (NaCl), pH 7.0.⁴² The DNA concentrations are expressed in molarity of base pairs and are indicated as C_p . Sodium chloride, sodium iodide and sodium cacodylate

(NaCac = $(\text{CH}_3)_2\text{AsOONa}$) were all analytical grade from Sigma-Aldrich and were used without further purification. Sodium chloride was used to adjust the ionic strength and sodium cacodylate (1.0×10^{-2} M) was employed to keep the pH of the solutions at the value of 7.0. Ultra-pure water from a MillyQ Millipore purification system was used throughout.

Methods Measurements of pH were made by a 713 Metrohm pH-meter equipped with a combined glass electrode.

Absorption data were recorded on a Shimadzu UV 2450 spectrophotometer and fluorescence data on a Perkin-Elmer LS 55 spectrofluorometer. Both instruments were equipped with jacketed cell holders, providing temperature control to within $\pm 0.1^\circ\text{C}$. DNA titrations were carried out by adding increasing amounts of the polynucleotide directly into the cell (1 cm path length) containing the dye solution (typically 5.2×10^{-5} M for absorbance, 1.0×10^{-5} M for fluorescence). The additions were made by a Hamilton micro syringe connected to a Mitutoyo micrometric screw; such system enables additions as small as $0.166 \mu\text{L}$. Absorbance titrations were analysed at $\lambda = 412$ nm, fluorescence titrations at $\lambda_{\text{ex}} = 450$ nm and $\lambda_{\text{em}} = 484$ nm. Experimental data were analysed by means of non-linear least-square fitting procedures performed by a JANDEL (AISN software) program. The fluorescence spectra were deconvoluted using the algorithm included in the Origin 8.0 software.

Viscosity measurements were performed on an semimicro-Ubbelodhe viscometer (Cannon) immersed in a thermostated water-bath maintained at $25.0 \pm 0.1^\circ\text{C}$. The flow time was measured with a digital stopwatch; mean values of at least triplicated measurements were used to evaluate the sample viscosity. To enhance data reliability and reproducibility, particular care was used to wash the viscosimeter capillary; the washing sequence (using ultrapure solvents and particulate-free gas) was water-acetone-water-ethanol- N_2 drying. To properly analyze the viscosity measurements, the relative viscosity was calculated using the equation (9) of the text.

Kinetic measurements were performed on a T-jump apparatus ($\Delta T = 2.7^\circ\text{C}$) made in our laboratory, which is based on the Rigler et al. prototype.⁴³ A Xenon lamp – monochromator system

was used as light source and suitable silica photodiodes (Hamamatsu S1336, Japan) were used to detect the signal as absorbance changes. Experiments on dye self-aggregation were done at $\lambda = 450$ nm, varying dye concentration in the range $C_D = 7.9 \times 10^{-6}$ M to 3.15×10^{-4} M. Experiments on TFT binding to DNA under conditions of low dye content and polymer excess were done at constant dye concentration ($C_D = 2.0 \times 10^{-6}$ M) and varying the DNA concentration under the conditions $C_D/C_P = 0.005$ to 0.45 . Experiments on TFT binding to DNA under conditions of high dye content and polymer deficiency were done at constant DNA concentration (7.7×10^{-5} M) and varying the dye concentration under the conditions $C_D/C_P = 0.80$ to 3.3 . The kinetic curves (mono- or bi-exponential) were collected by an Agilent 54662A (Agilent Technologies, U.S.A.) digital oscilloscope, transferred to a PC and evaluated with a mathematical interpolation program, which yields the amplitudes and time constants of the exponential functions representing the kinetic behaviour. It should be pointed out that the output of the instrument is such that descending curves correspond to positive amplitudes. Each experiment was repeated at least ten times and the values of the time constants and amplitudes are averaged values (spread $\leq 1\%$ for the experiments with TFT alone, spread $\leq 10\%$ for the experiments with TFT+DNA).

Molecular dynamics of TFT in explicit water As no experimental structures are available for TFT bound to dsDNA's we have derived structures performing hybrid QM/MM MD simulations of the intercalated monomer and of a minor groove bound dimer. TFT was represented using the general AMBER force field (GAFF),⁴⁴ while RESP charges have been obtained performing a quantum chemistry calculation on the isolated molecule using Gaussian09.⁴⁵ Water molecules were represented by the TIP3P model and DNA was simulated using the AMBER parm99/bsc0 force field.⁴⁶ DNA was represented by a B-DNA dodecamer, generated using the nucgen module of AMBER and having the sequence d(ATATATATATAT)₂. The initial conformation of the TFT–DNA complexes was simulated in a truncated octahedron with periodic boundary conditions. Sodium ions were added to the system to neutralize the charge. The solute was surrounded by

roughly 5700 TIP3P water molecules, leaving about 10 Å space between the solute and the faces of the box. In all MD trajectories we considered a cut-off of 9.0 Å, and Ewald particle mesh algorithm was used to evaluate electrostatic interactions.⁴⁷ Bonds to hydrogen atoms were fixed with the SHAKE algorithm.⁴⁸ Temperature was controlled using the Langevin algorithm⁴⁹ with collision frequency of 2 ps⁻¹.⁵⁰ QM/MM MD simulations⁵¹ with periodic boundary conditions were performed using SANDER which is part of the AMBER12 suite of programs.⁴⁹ The QM region was described by the PM6 method⁵² with an empirical dispersion correction (PM6-D).⁵³ The SHAKE algorithm was used to restrain the bonds containing hydrogen in both QM and MM regions, allowing a time step of 2 fs to be used.⁵⁴ After a full MM energy minimization, the system was equilibrated at 300 K for 1 ns using constant volume and temperature (nVT) and then by constant pressure and temperature (nPT) to 1 bar pressure using the QM/MM MD with the TFT now treated quantum mechanically.

References

- 1 A. I. Sulatskaya, A. A. Maskevich, I. M. Kuznetsova, V. N. Uversky and K. K. Turoverov, *Plos One*, 2010, **5**.
- 2 N. Amdursky, Y. Erez and D. Huppert, *Accounts Chem. Res.*, 2012, **45**, 1548-1557.
- 3 V. I. Stsiapura, A. A. Maskevich, V. A. Kuzmitsky, K. K. Turoverov and I. M. Kuznetsova, *J. Phys. Chem. A*, 2007, **111**, 4829-4835.
- 4 P. S. Vassar, C. F. A. Culling and H. E. Taylor, *Am. J. Pathol.*, 1959, **35**, 718.
- 5 T. I. Mandybur, *Neurology*, 1975, **25**, 120-126.
- 6 H. Naiki, K. Higuchi, M. Hosokawa and T. Takeda, *Anal. Biochem.*, 1989, **177**, 244-249.
- 7 T. Ban, D. Hamada, K. Hasegawa, H. Naiki and Y. Goto, *J. Biol. Chem.*, 2003, **278**, 16462-16465.
- 8 M. Biancalana and S. Koide, *Bioch. Biophys. Acta*, 2010, **1804**, 1405-1412.
- 9 T. G. Deligeorgiev, S. Kaloyanova and J. J. Vaquero, *Recent Pat. Mater. Sci.*, 2009, **2**, 1-26; T. Biver, M. Pulzonetti, F. Secco, M. Venturini and S. Yarmoluk, *Arch. Biochem. Biophys.*, 2006, **451**, 103-111; T. Biver, B. Garcia, J. M. Leal, F. Secco and E. Turriani, *Phys. Chem. Chem. Phys.*, 2010, **12**, 13309-13317; A. Biancardi, T. Biver, A. Marini, B. Mennucci and F. Secco, *Phys. Chem. Chem. Phys.*, 2011, **13**, 12595-12602.
- 10 B. A. Armitage, *Top. Curr. Chem.*, 2005, **253**, 55-76.
- 11 T. Biver, A. De Biasi, F. Secco, M. Venturini and S. Yarmoluk, *Biophys. J.*, 2005, **89**, 374-383.
- 12 M. Ilanchelian and R. Ramaraj, *J. Photochem. Photobiol. A*, 2004, **162**, 129-137.
- 13 R. B. Cundall, A. K. Davies, P. G. Morris and J. Williams, *J. Photochem.*, 1981, **17**, 369-376.
- 14 T. Biver, A. Boggioni, F. Secco, E. Turriani, M. Venturini and S. Yarnaoluk, *Arch. Biochem. Biophys.*, 2007, **465**, 90-100.
- 15 R. Steiger, R. Pugin and J. Heier, *Colloids Surf. B*, 2009, **74**, 484-491.
- 16 R. Schirra, *Chem. Phys. Lett.*, 1985, **119**, 463-466.
- 17 A. I. Novaira and C. M. Previtali, *J. Photochem. Photobiol. B*, 2006, **85**, 102-108.
- 18 E. R. Carraway, J. N. Demas, B. A. Degraff and J. R. Bacon, *Anal. Chem.*, 1991, **63**, 337-342; J. R. Lakowicz, *Principles of Fluorescence Spectroscopy.*, Plenum Press, **1983**.
- 19 J. T. Petty, J. A. Bordelon and M. E. Robertson, *J. Phys. Chem. B*, 2000, **104**, 7221-7227.
- 20 T. Biver, *Appl. Spectrosc. Rev.*, 2012, **47**, 272-325.
- 21 T. Biver, F. Secco and M. Venturini, *Arch. Biochem. Biophys.*, 2005, **437**, 215-223.
- 22 M. T. Record, C. F. Anderson and T. M. Lohman, *Q. Rev. Biophys.*, 1978, **11**, 103-178.
- 23 G. Scatchard, *Ann. N. Y. Acad. Sci.*, 1949, **51**, 660-672.
- 24 J. D. McGhee and H. Von, Peter H., *J. Mol. Biol.*, 1974, **86**, 469-489.
- 25 D. Suh and J. B. Chaires, *Bioorgan. Med. Chem.*, 1995, **3**, 723-728.
- 26 G. Cohen and H. Eisenberg, *Biopolymers*, 1969, **8**, 45-55.
- 27 F. Secco and M. Venturini, *J. Chem. Soc., Faraday Trans.*, 1993, **89**, 719-725.
- 28 A. S. Tatikolov, *J. Photochem. Photobiol. C*, 2012, **13**, 55-90.
- 29 M. M. Wang, G. L. Silva and B. A. Armitage, *J. Am. Chem. Soc.*, 2000, **122**, 9977-9986.
- 30 P. L. Brezonik, CRC Press LLC, Boca Raton, Florida, **2002**, p. 155.
- 31 H. Boaz and G. K. Rollefson, *J. Am. Chem. Soc.*, 1950, **72**, 3435-3443.
- 32 L. S. Lerman, *J. Mol. Biol.*, 1961, **3**, 18-30.
- 33 J. B. Chaires, *Arch. Biochem. Biophys.*, 2006, **453**, 26-31.
- 34 J. L. Bresloff and D. M. Crothers, *J. Mol. Biol.*, 1975, **95**, 103-&.
- 35 T. Biver, F. Secco and M. Venturini, *Coordin. Chem. Rev.*, 2008, **252**, 1163-1177.
- 36 S. Y. Breusegem, R. M. Clegg and F. G. Loontjens, *J. Mol. Biol.*, 2002, **315**, 1049-1061.
- 37 F. J. Meyer-Almes and D. Porschke, *Biochemistry-Us*, 1993, **32**, 4246-4253.
- 38 T. Biver, F. Secco, M. R. Tine, M. Venturini, A. Bencini, A. Bianchi and C. Giorgi, *J. Inorg. Biochem.*, 2004, **98**, 1531-1538.
- 39 L. Liu, Y. Shao, J. Peng, H. Liu and L. Zhang, *Molecular BioSystems*, 2013, **9**, 2512-2519.
- 40 M. R. Beccia, T. Biver, A. Pardini, J. Spinelli, F. Secco, M. Venturini, N. B. Vazquez, M. P. L. Cornejo, V. I. M. Herrera and R. P. Gotor, *Chem-Asian J.*, 2012, **7**, 1803-1810.
- 41 T. Biver, D. Lombardi, F. Secco, M. R. Tiné, M. Venturini, A. Bencini, A. Bianchi and B. Valtancoli, *Dalton Transactions*, 2006, 1524-1533.
- 42 G. Felsenfeld and S. Z. Hirschman, *Journal of Molecular Biology*, 1965, **13**, 407-427.

- 43 R. Rigler, C. R. Rabl and T. M. Jovin, *Review of Scientific Instruments*, 1974, **45**, 580-588.
- 44 AMBER 12, D.A. Case, T.A. Darden, T.E. Cheatham III, C.L. Simmerling, J. Wang, R.E. Duke, R. Luo, R.C. Walker, W. Zhang, K.M. Merz, B. Roberts, S. Hayik, A. Roitberg, G. Seabra, J. Swails, A.W. Götz, I. Kolossváry, K.F. Wong, F. Paesani, J. Vanicek, R.M. Wolf, J. Liu, X. Wu, S.R. Brozell, T. Steinbrecher, H. Gohlke, Q. Cai, X. Ye, J. Wang, M.-J. Hsieh, G. Cui, D.R. Roe, D.H. Mathews, M.G. Seetin, R. Salomon-Ferrer, C. Sagui, V. Babin, T. Luchko, S. Gusarov, A. Kovalenko and P. A. Kollman, **2012**, University of California - San Francisco,
- 45 Gaussian 09, Revision H.11, M. J. Frisch, G. W. Trucks, H. B. Schlegel, G. E. Scuseria, M. A. Robb, J. R. Cheeseman, G. Scalmani, V. Barone, B. Mennucci, G. A. Petersson, H. Nakatsuji, M. Caricato, X. Li, H. P. Hratchian, A. F. Izmaylov, J. Bloino, G. Zheng, J. L. Sonnenberg, M. Hada, M. Ehara, K. Toyota, R. Fukuda, J. Hasegawa, M. Ishida, T. Nakajima, Y. Honda, O. Kitao, H. Nakai, T. Vreven, J. Montgomery, J. A., J. E. Peralta, F. Ogliaro, M. Bearpark, J. J. Heyd, E. Brothers, K. N. Kudin, V. N. Staroverov, R. Kobayashi, J. Normand, K. R. Raghavachari, T. Nakajima, Y. Honda, O. Kitao, H. Nakai, T. Vreven, J. Montgomery, J. A., J. E. Peralta, F. Ogliaro, M. Bearpark, J. J. Heyd, E. Brothers, K. N. Kudin, V. N. Staroverov, R. Kobayashi, J. Normand, K. Raghavachari, A. Rendell, J. C. Burant, S. S. Iyengar, J. Tomasi, M. Cossi, N. Rega, J. M. Millam, M. Klene, J. E. Knox, J. B. Cross, V. Bakken, C. Adamo, J. Jaramillo, R. Gomperts, R. E. Stratmann, O. Yazyev, A. J. Austin, R. Cammi, C. Pomelli, J. W. Ochterski, R. L. Martin, K. Morokuma, V. G. Zakrzewski, G. A. Voth, P. Salvador, J. J. Dannenberg, S. Dapprich, A. D. Daniels, Ö. Farkas, J. B. Foresman, J. V. Ortiz, J. Cioslowski and D. J. Fox, **2009**, Wallingford CT, Gaussian Inc.
- 46 J. M. Wang, P. Cieplak and P. A. Kollman, *J. Comput. Chem.*, 2000, **21**, 1049-1074; A. Perez, I. Marchan, D. Svozil, J. Sponer, T. E. Cheatham, C. A. Laughton and M. Orozco, *Biophys. J.*, 2007, **92**, 3817-3829; A. T. Guy, T. J. Piggot and S. Khalid, *Biophys. J.*, 2012, **103**, 1028-1036.
- 47 T. Darden, D. York and L. Pedersen, *J. Chem. Phys.*, 1993, **98**, 10089-10092; U. Essmann, L. Perera, M. L. Berkowitz, T. Darden, H. Lee and L. G. Pedersen, *J. Chem. Phys.*, 1995, **103**, 8577-8593.
- 48 J. P. Ryckaert, G. Ciccotti and H. J. C. Berendsen, *J. Comput. Phys.*, 1977, **23**, 327-341; S. Miyamoto and P. A. Kollman, *J. Comput. Chem.*, 1992, **13**, 952-962.
- 49 S. Q. He and H. A. Scheraga, *J. Chem. Phys.*, 1998, **108**, 271-286.
- 50 D. A. Case, T. E. Cheatham, T. Darden, H. Gohlke, R. Luo, K. M. Merz, A. Onufriev, C. Simmerling, B. Wang and R. J. Woods, *J. Comput. Chem.*, 2005, **26**, 1668-1688.
- 51 R. C. Walker, M. F. Crowley and D. A. Case, *J. Comput. Chem.*, 2008, **29**, 1019-1031.
- 52 J. J. P. Stewart, *J. Mol. Model.*, 2007, **13**, 1173-1213.
- 53 P. Jurecka, J. Cerny, P. Hobza and D. R. Salahub, *J. Comput. Chem.*, 2007, **28**, 555-569.
- 54 G. D. Seabra, R. C. Walker, M. Elstner, D. A. Case and A. E. Roitberg, *J. Phys. Chem. A*, 2007, **111**, 5655-5664.

